Int J Thermophys (2012) 33:2159–2166
DOI 10.1007/s10765-012-1218-9

Phase Transitions at Low Temperature (<77 K) by Means of Photopyroelectric Calorimetry

A. Oleaga · A. Salazar

Received: 13 January 2012 / Accepted: 11 May 2012 / Published online: 24 May 2012

Abstract An ac photopyroelectric calorimeter has been designed and mounted to work at low temperatures (12 K to 77 K), where the sample is in a He atmosphere and with the detector region isolated from mechanical vibrations allowing the retrieval of high resolution measurements of thermal diffusivity and specific heat. The system has been used to study magnetic and ferroelectric phase transitions in $RMnO_3$ (R = Sm, Tb, Dy). The high quality of the measurements has allowed study of the critical behavior of the transitions and extraction of their critical parameters. In the particular case of the antiferromagnetic-to-paramagnetic transition in $SmMnO_3$, it belongs to the 3D-XY universality class while in the case of the lock-in, ferroelectric transition in $TbMnO_3$, the results confirm that the transition is clearly second order.

Keywords Calorimetry · Low temperatures · Manganites · Photopyroelectric · Thermal diffusivity

1 Introduction

1.1 Photopyroelectric Calorimetry in the Back Configuration

High resolution ac photopyroelectric (PPE) calorimetry has been successfully used to extract thermal properties from both solid and liquid materials. In particular, using the standard back-detection configuration [1,2], simultaneous measurements of the thermal conductivity K, thermal diffusivity D, and specific heat c_p can be carried out. As performed in our lab for the case of solid materials, in this configuration an

A. Oleaga (✉) · A. Salazar
Departamento de Física Aplicada I, Escuela Técnica Superior de Ingeniería, Universidad del País Vasco, Alameda Urquijo s/n, 48013 Bilbao, Spain
e-mail: alberto.oleaga@ehu.es

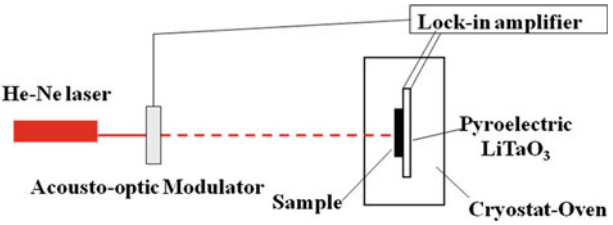

Fig. 1 Standard back configuration of a photopyroelectric calorimeter

acousto-optically modulated He–Ne laser beam of 5 mW illuminates the front surface of the sample under study (see Fig. 1). Its rear surface is in thermal contact with a 350 μm thick $LiTaO_3$ pyroelectric detector with Ni–Cr electrodes on both surfaces, by using an extremely thin layer of a highly heat-conductive silicone grease (Dow Corning 340 heat sink compound). The PPE signal is processed by a lock-in amplifier operating in the current mode. Both sample and detector are placed inside a nitrogen bath cryostat or an oven, depending on the temperature range of study (77 K to 650 K). Measurements are performed at rates that vary from 100 $\mathrm{mK \cdot min^{-1}}$ for measurements on a wide temperature range to 10 $\mathrm{mK \cdot min^{-1}}$ (or even lower) for high resolution runs close to the phase transitions.

For opaque and thermally thick samples (i.e., the thickness of the sample is higher than the thermal diffusion length $\mu = \sqrt{D/\pi f}$, where f is the modulation frequency of the laser beam), the natural logarithm ($\ln V$) of the amplitude of the normalized PPE signal (which is obtained by dividing the measured signal by the signal provided by the bare detector) and its phase (Ψ) have a linear dependence on $\sqrt{f}$, with the same slope. From their slope m and from the vertical separation between the two straight lines d, the thermal diffusivity and the thermal effusivity ($e = \sqrt{\rho c_p K} = K/\sqrt{D}$) of the sample can be obtained [3];

$$D = \frac{\pi \ell^2}{m^2}, \tag{1}$$

$$e = e_{\mathrm{p}} \left(\frac{2}{\exp(d)} - 1 \right), \tag{2}$$

where ρ is the density, ℓ is the sample thickness, and e_{p} is the thermal effusivity of the pyroelectric detector.

Once the thermal diffusivity and effusivity have been measured at a certain reference temperature (T_{ref}, D_{ref}, e_{ref}), the temperature is changed while recording the amplitude and phase of the pyroelectric signal, at a fixed frequency. The temperature dependence of D and e are given by [3,4]

$$D(T) = \left(\frac{1}{\sqrt{D_{\mathrm{ref}}}} - \frac{\Delta(T)}{\ell \sqrt{\pi f}} \right)^{-2} \tag{3}$$

$$e(T) = e_{\mathrm{p}}(T) \left(\frac{1 + \frac{e_{\mathrm{ref}}}{e_{\mathrm{p}}(T_{\mathrm{ref}})}}{\exp[\Delta''(T)]} - 1 \right), \tag{4}$$

where $\Delta(T) = \Psi(T) - \Psi(T_{\text{ref}})$, $\Delta'(T) = \ln V(T) - \ln V(T_{\text{ref}})$, and $\Delta''(T) = \Delta'(T) - \Delta(T)$. Finally, the temperature dependence of the specific heat and thermal conductivity are calculated from the following relations:

$$c_p(T) = \frac{e(T)}{\rho\sqrt{D(T)}} \tag{5}$$

$$K(T) = e(T)\sqrt{D(T)} \tag{6}$$

This technique is specially suited to study the critical behavior of phase transitions as small temperature gradients in the sample give rise to a high signal-to-noise ratio in the detector, so the features of the transition in the near vicinity of the critical temperature can be studied with great detail. The usefulness of this technique has been well demonstrated in the study of the critical behavior of second-order magnetic and ferroelectric transitions in different materials, for instance: Cr_2O_3 [5], NiO [6], $KMnF_3$[7], $La_{1-x}Sr_xO_3$ [8], $Sn_2P_2(S_{1-x}Se_x)_6$ [9]. Besides, it has also proved to be a precise technique to ascertain the character of phase transitions, evaluating the latent heat in the case of first-order ones: liquid crystals [10], CoO [11]. See Ref. [12] for a whole review of its applications.

1.2 Low Temperature Measurements

77 K is the usual lower limit for PPE calorimetry at any lab, while it is evident that it is interesting to extend the capabilities of this calorimetry to lower temperatures. In order to be able to extend our working temperature range, some years ago a commercial closed cycle He cryostat was incorporated to our lab and the sample holder adapted for PPE calorimetry. Before, very few low temperature measurements performed with this calorimetry could be found in the literature and none of them of high resolution [13], which is imperative in order to study phase transitions in detail. The characteristics of our commercial system were that the sample was kept in vacuum and cooled by means of a cold finger. The main advantage of a closed cycle system is that there is no liquid He consumption, which is too expensive. But there were strong difficulties in the system, since the temperature was lowered by means of a mechanical device which introduced vibrations on the sample holder and the detector, affecting the PPE signal (the pyroelectric sensor is piezoelectric as well). On the other hand, as the temperature decreases, the thermal coupling between the sample and the pyroelectric sensor is reduced (the sample is in vacuum) and therefore the thermal diffusivity is underestimated while the specific heat is overestimated. After having thoroughly studied both problems and tested different experimental conditions, we were able to minimize those difficulties to study the antiferromagnetic-to-paramagnetic transition in $SmMnO_3$ [14], but it was not a system easy to work with. So we decided to try to overcome these two problems designing a new system in which there were no mechanical vibrations transmitted to the detector and the sample were not in vacuum. Janis Corporation had a Mossbauer closed cycle He system which fulfilled both conditions and, in collaboration with the company, particular adaptations to that system were designed and performed to work as a PPE calorimeter. In this new sys-

tem the detector and sample are completely isolated from the refrigerating rotor and it works in a helium atmosphere, so the thermal coupling is maintained over the whole temperature range which is 12 K to 320 K, allowing minimal cooling/heating rates down to even $5\,\mathrm{mK}\cdot\mathrm{min}^{-1}$.

The aim of this work is to present this new system by measuring the thermal properties of a series of manganites, one of which has already been studied with the older system (as a test) and some other new compounds with phase transitions at low temperatures. The work will be completed with the study of the critical behavior of some of the second-order phase transitions found in the samples.

2 Samples Studied: Manganites

Manganites $R_{1-x}A_xMnO_3$ (R = lanthanide, A = alkaline earth) attracted great attention at the end of the 1990s because of their colossal magnetoresistance [15]; afterwards, they have become a research field of their own in solid-state physics because of the strong interplays between magnetism, electron-lattice coupling, and orbital and charge ordering, which have been revealed as the phase diagrams of the different families and combinations have been obtained and the physical properties studied by many techniques. In particular, the properties of the parent compounds $RMnO_3$ strongly depend on the R ion. As the atomic number is increased, from R = La to Dy they crystallize in an orthorhombic system, while from then on (Ho to Lu), they are hexagonal. This work is focused on the orthorhombic samples, of which we had already studied La, Pr, Nd, and Sm [14,16]. We have studied again $SmMnO_3$ as a control and have added $TbMnO_3$ and $DyMnO_3$, which have a rich phase diagram at low temperature [17]. Both of them are known to have a geometrically frustrated paramagnetic-to-antiferromagnetic transition at temperatures lower than 50 K, giving rise to an incommensurate low temperature phase. At a lower temperature there is in both cases a lock-in transition (from incommensurate to commensurate) which is also ferroelectric.

All the samples used in this study are high quality single crystals grown by the floating-zone technique and slices of thicknesses of about 0.35 mm to 0.45 mm were used for the study. The surfaces of the samples were cut perpendicular to the *c*-axis.

3 Experimental Results and Fittings

3.1 Thermal Diffusivity and Specific Heat

The thermal diffusivities of the three manganites are shown in Fig. 2. The general behavior with respect to temperature is typical of insulating systems, where phonons are responsible for heat transport. From a high value at low temperature, it quickly decreases as the temperature is raised because of the reduction in the phonon mean free path. The transitions are observed as severe dips in the thermal diffusivity curve, and after the antiferromagnetic-to-paramagnetic transitions (59.3 K for Sm, 40.9 K for Tb and 38.1 K for Dy), the reduction is softer, as happens with La, Pr, and Nd [16] but steady until they reach room temperature values.

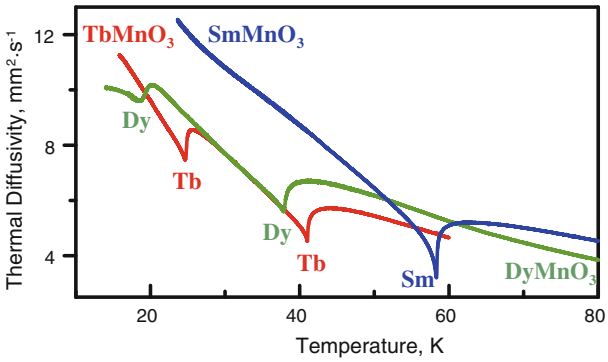

Fig. 2 Thermal diffusivity as a function of temperature, at low temperatures, for $RMnO_3$ (R = Sm, Tb, Dy)

These have also been measured and have resulted in the following values: $1.29\,\mathrm{mm}^2 \cdot \mathrm{s}^{-1}$ for Sm, $1.28\,\mathrm{mm}^2 \cdot \mathrm{s}^{-1}$ for Tb, and $1.09\ \mathrm{mm}^2 \cdot \mathrm{s}^{-1}$ for Dy.

The transitions at very low temperature observed in Fig. 2 (24.6 K for Tb and 18.6 K for Dy) correspond to the lock-in transitions cited in the literature [17]. The experimental curves are composed of thousands of points, since the measurements were performed at very low rates (down to $10\,\mathrm{mK} \cdot \mathrm{min}^{-1}$); the frequencies at which the measurements have been performed have been chosen so that the thermally thick regime is attained (between 13 Hz and 35 Hz depending on the particular samples). It is worth noting that the measured values for $SmMnO_3$ agree with our previous measurements with the older system but the curve is of a higher quality than before [14].

Figure 3 shows the obtained specific heat for the case of $TbMnO_3$ where we can appreciate that the curve is a little bit noisier than in the case of the thermal diffusivity. This is because the thermal diffusivity is obtained using only the phase of the electric signal (which is extremely stable) while for extracting the specific heat, both the amplitude and phase are needed. In the first place, the amplitude is always somewhat noisier and, besides, the way the amplitude and phase enter in Eq. 5 makes the specific heat not be as clean as the thermal diffusivity. Nevertheless, the curves are of high quality.

3.2 Critical Behavior

In this section and as a proof of the resolution of the measurements in order to extract quantitative information from the experimental curves, we concentrate on the study of the critical behavior of the specific heat in second-order phase transitions, which are described by a function of the form,

$$c_p = B + Ct + A^{\pm} |t|^{-\alpha} \left(1 + E^{\pm} |t|^{0.5}\right), \tag{7}$$

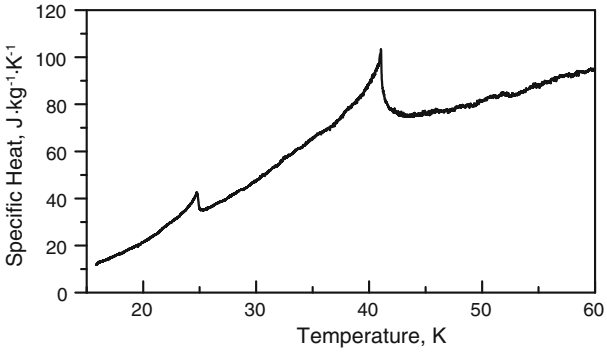

Fig. 3 Specific heat as a function of temperature for $TbMnO_3$

where $t = (T - T_C)/T_C$ is the reduced temperature, T_C is the critical temperature, and α, $A^{\pm}$, B, C, and $E^{\pm}$ are adjustable parameters. Superscripts + and − stand for $T > T_C$ and $T < T_C$, respectively. The linear term represents the background contribution to the specific heat, while the last term is the anomalous contribution to the specific heat. The factor under the parenthesis is the correction to scaling that represents a singular contribution to the leading power as known from experiments and theory [5,18].

The experimental data were simultaneously fitted for $T > T_C$ and $T < T_C$ with a nonlinear least-squares routine using a Levenberg–Marquardt method. First of all, we selected a fitting range close to the dip while avoiding the rounding, and kept the value of T_C fixed. We obtained a first fit without a correction to the scaling term and obtained a set of adjustable parameters. Afterwards, we tried to increase the number of points included in the fit, first fixing t_{min} and increasing t_{max}, and then fixing t_{max} and decreasing t_{min}. The next step was introducing the correction to the scaling term trying to improve the fit. As a last check, we let T_C be a free parameter in order to confirm the fit. In the whole process, we focused our attention on the root-mean-square values as well as on the deviation plots, which are the plots of the differences between the fitted values and the measured ones as a function of the reduced temperature.

As an example, we present the fit of the magnetic transition in $SmMnO_3$ and the ferroelectric transition in $TbMnO_3$. In Fig. 4, a close-up of these transitions in the near vicinity of the respective critical temperatures are presented. The dots correspond to the experimental points (not all of them have been presented, for the sake of clarity) and the continuous lines to the best fit in both cases, which are very good.

In the case of $SmMnO_3$, the best fit has given the values $\alpha = -0.011$ and $A^+/A^- = 1.03$, using a reduced temperature range of 8.25×10^{-2} to 1.9×10^{-3} for $T < T_N$ and 2.4×10^{-4} to 8.6×10^{-2} for $T > T_N$. The values of the critical parameters clearly indicate that this manganite belongs to the 3D-XY universality class (theoretical values $\alpha = -0.014$, $A^+/A^- = 1.06$).

In the case of $TbMnO_3$ the best fit has given the values $\alpha = -0.087$ and $A^+/A^- = 1.45$, using a reduced temperature range of 1.9×10^{-1} to 5.31×10^{-3} for $T < T_C$ and 2.0×10^{-4} to 1.9×10^{-1} for $T > T_C$. As this is a lock-in transition as well as a ferroelectric transition, there has been some debate whether the character of the

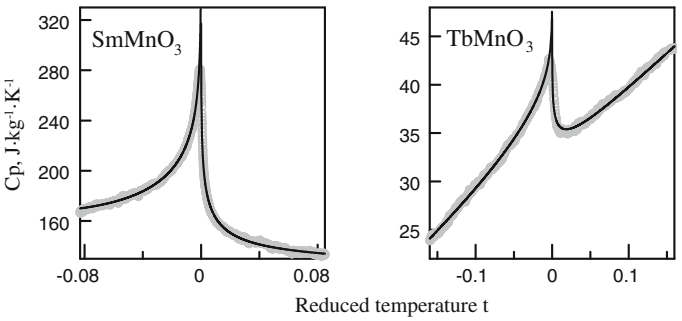

Fig. 4 Experimental (*dots*) and *fitted curves* (*continuous lines*) of the specific heat as a function of the reduced temperature for the antiferromagnetic-to-paramagnetic transition in $SmMnO_3$ (T_N = 59.3 K) and the lock-in, ferroelectric transition in $TbMnO_3$ (T_C = 24.6 K)

transition could be first order as in $GdMnO_3$ [19] but the results correspond very well with a second-order phase transition, close to the values of the Heisenberg universality class ($\alpha = -0.11$, $A^+/A^- = 1.5$), so the possibility of a first-order character is discarded.

4 Conclusions

An ac PPE calorimeter has been designed and mounted to work at low temperatures (12 K to 77 K), where the sample is in a He atmosphere and with the sample/detector region isolated from the mechanical vibrations produced by the cooling head, allowing acquisition of high resolution measurements of thermal diffusivity and specific heat. The system has been used to study magnetic and ferroelectric phase transitions in $RMnO_3$ (R = Sm, Tb, Dy). The high quality of the measurements has allowed study of the critical behavior of the transitions and extraction of their critical parameters. In the particular case of the antiferromagnetic-to-paramagnetic transition in $SmMnO_3$, it belongs to the 3D-XY universality class while in the case of the lock-in, ferroelectric transition in $TbMnO_3$, the transition is clearly second order, with critical parameters close to the Heisenberg class.

Acknowledgments This work has been supported by the Ministerio de Ciencia e Innovación (MAT2011-23811) and by Gobierno Vasco (IT351-10).

References

1. M. Marinelli, U. Zammit, F. Mercuri, R. Pizzoferrato, J. Appl. Phys. **72**, 1096 (1992)
2. M. Chirtoc, D. Dadarlat, D. Bicanic, J.S. Antoniow, M. Egée, in *Progress in Photothermal and Photoacoustic Science and Technology*, vol. 3, ed. by A. Mandelis, P. Hess (SPIE, Bellingham, 1997)
3. S. Delenclos, M. Chirtoc, A. Hadj Sahraoui, C. Kolinsky, J.M. Buisine, Rev. Sci. Instrum. **73**, 2773 (2002)
4. A. Salazar, Rev. Sci. Instrum. **74**, 825 (2003)
5. M. Marinelli, F. Mercuri, U. Zammit, R. Pizzoferrato, F. Scudieri, D. Dadarlat, Phys. Rev. B **49**, 9523 (1994)

6. A. Salazar, M. Massot, A. Oleaga, A. Pawlak, W. Schranz, Phys. Rev. B **75**, 224428 (2007)
7. M. Massot, A. Oleaga, A. Salazar, D. Prabhakaran, M. Martin, P. Berthet, G. Dhalenne, Phys. Rev. B **77**, 134438 (2008)
8. A. Oleaga, A. Salazar, D. Prabhakaran, A.T. Boothroyd, Phys. Rev. B **70**, 184402 (2004)
9. A. Oleaga, A. Salazar, A.A. Kohutych, Yu.M. Vysochanskii, J. Phys. Condens. Matter **23**, 025902 (2011)
10. F. Mercuri, M. Marinelli, S. Paoloni, U. Zammit, F. Scudieri, Appl. Phys. Lett. **92**, 251911 (2008)
11. A. Oleaga, A. Salazar, E.H. Bocanegra, Phys. Rev. B **80**, 024426 (2009)
12. U. Zammit, M. Marinelli, F. Mercuri, S. Paoloni, F. Scudieri, Rev. Sci. Instrum. **82**, 121101 (2011)
13. M. Chirtoc, D. Giese, B. Arnscheidt, N. Kalevich, J. Pelzl, Opt. Eng. B **36**, 303 (1997)
14. M. Massot, A. Oleaga, A. Salazar, Meas. Sci. Technol. **17**, 3245 (2006)
15. Y. Tokura, Y. Tomioka, J. Magn. Magn. Mater. **200**, 1 (1999)
16. A. Oleaga, A. Salazar, D. Prabhakaran, A.T. Boothroyd, J. Phys. Condens. Matter **17**, 6729 (2005)
17. T. Kimura, S. Ishihara, H. Shintani, T. Arima, K.T. Takahashi, K. Ishizaka, Y. Tokura, Phys. Rev. B **68**, 060403(R) (2003)
18. A. Kornblit, G. Ahlers, Phys. Rev. B **11**, 2678 (1975)
19. K. Noda, S. Nakamura, J. Nagayama, H. Kuwahara, J. Appl. Phys. **97**, 10C103 (2005)